American Journal of Physics

PAPERS | NOVEMBER 01 2022

Using Hexbugs™ to model gas pressure and electrical conduction: A pandemic-inspired distance lab

Genevieve DiBari; Liliana Valle; Refilwe Tanah Bua; Lucas Cunningham; Eleanor Hort; Taylor Venenciano; Janice Hudgings

Am. J. Phys. 90, 817–825 (2022)
https://doi.org/10.1119/5.0087142

AAPT PHYSICS EDUCATION®

Using Hexbugs™ to model gas pressure and electrical conduction: A pandemic-inspired distance lab

Genevieve DiBari,[a] Liliana Valle,[a),b)] Refilwe Tanah Bua,[c)] Lucas Cunningham, Eleanor Hort, Taylor Venenciano,[d)] and Janice Hudgings[e)]
Physics and Astronomy Department, Pomona College, Claremont, California 91711

(Received 1 February 2022; accepted 9 September 2022)

We describe a pandemic-inspired, modern physics distance lab course, focused both on engaging undergraduate physics majors in scientific research from their homes and on building skills in scientific paper reading and writing. To introduce the experimental and analytic tools, students are first asked to complete a traditional lab assignment in which collections of Hexbugs™, randomly moving toy automatons, are used to model gas molecules and to confirm the ideal gas law. Subsequently, after consulting the literature, students propose and implement semester-long experiments using Hexbugs™, smartphones, and materials commonly found at home to model various concepts in statistical mechanics and electrical conduction. A sample project focused on the Drude model, in which Hexbugs™ on a tilted plane are used to model electrical conduction, is described in detail. Alongside the research projects, students write formal, peer-reviewed scientific papers on their work, modeling the professional publication process as closely as possible. Somewhat paradoxically, we found that the pandemic-inspired exigency of reliance on simple, home-built experiments enabled an increased focus on developing experimental research skills and achieving the laboratory learning objectives recommended by the American Association of Physics Teachers.
https://doi.org/10.1119/5.0087142

I. INTRODUCTION

Recent years have seen an explosion of academic and commercial interest in the development of online instructional lab exercises due both to the COVID-19 pandemic and to the rapid growth in online education in its own right. While the pandemic forced a rapid, unplanned-for transition from in-person labs to online labs at many institutions, a recent survey of the response of physics programs across the United States found that "For some instructors, the move to remote/hybrid teaching may be a unique opportunity to transform the lab course—rethinking learning goals, implementing course-based undergraduate research experiences (CURES), having at-home maker spaces or labs that focus heavily on experimental design, and modeling to increase student agency, or completely restructuring both the lectures and labs to have investigative science learning environments (ISLEs)."[1] In this work, we describe just such an initiative: a pandemic-inspired rethinking of a sophomore-level modern physics lab course, including re-examining the learning objectives and developing a hands-on laboratory experience enabling students to conduct original physics research from home.

The American Association of Physics Teachers (AAPT) recommends six learning outcome focus areas for lab courses: "constructing knowledge," "modeling," "designing experiments," "developing technical and practical laboratory skills," "analyzing and visualizing data," and "communicating physics."[2] These focus areas are summarized with additional details in supplementary material Table 1.[3] By de-emphasizing the use of sophisticated equipment, the at-home lab course described in this paper focuses more directly on AAPT-recommended learning objectives centered on the development of experimental skills, including reading the scientific literature; selecting a research question; designing, implementing, and debugging an experimental apparatus; data analysis; modeling; and scientific communication.

In this paper, we describe the structure of the lab course and then present two of the experiments in detail, highlighting the use of Hexbugs™, commonly available, inexpensive toy automatons that exhibit semi-random motion,[4] to model phenomena in statistical mechanics and electrical conduction. We note that, while originally developed for an online modern physics lab course, the experiments described here might also be useful for instructional labs or lecture demonstrations in statistical mechanics, physical chemistry, biophysics, or introductory electromagnetism, either online or in-person.

II. GENERAL STRUCTURE OF THE LAB COURSE

The online distance lab course described in this paper is attached to a relatively standard undergraduate modern physics course that is required of all physics and astronomy majors at our college and typically taken in a student's sophomore or junior year. The course enrolls roughly 20 students per year but is scalable to larger numbers. Whereas the in-person version of the lab previously focused largely on benchtop quantum optics experiments, the online version discussed here is centered on statistical mechanics experiments using Hexbugs™. The inspiration for these experiments is largely drawn from prior publications illustrating the use of Squiggle-Balls™ in instructional laboratories.[5–7] The semi-randomly moving Hexbugs™[8] can be used to model the behavior of particles such as gas molecules, electrons in a diffusive medium, or any object subject to a random walk, including more complex behaviors in the subfields of active matter and granular materials.[9–19] In this lab course, we focus on using Hexbugs™ to conduct quantitative, macro-scale explorations of otherwise microscale behavior that can be difficult for students to visualize, including an exploration of the ideal gas law, electrical conduction, and more.

Table I. Structure of the online modern physics lab course.

Week	Technical focus	Scientific communication focus
1–3	Computational modeling and introduction to MATHEMATICA and MATLAB	Reading "How to Read Scientific Papers" by Schmidl[24]
4	Conventional structured lab: using Hexbugs™ to model gas pressure	Reading "Experiments in statistical mechanics" by Prentis[6]
5	Reading literature; brainstorming experimental research questions	Reading curated selection of experimental research papers[6,7,9–12,22]
6	Research proposal	Reverse outlining a scientific paper
7–9	Designing, building, and debugging experiment; data collection	Drafting and revising sections of manuscript: introduction, experimental methods, and theory
10–11	Data analysis and modeling	Drafting and revising sections of manuscript: results, discussion, conclusion, abstract, acknowledgements
12	None	Anonymous peer review of manuscripts
13	None	Revised final manuscript and responses to reviewers due

The overall structure of the lab course is summarized in Table I. The first three weeks focus on introducing students to MATHEMATICA[20] and MATLAB,[21] tools that are used throughout the lab course for computational modeling and data analysis. In order to build basic familiarity with the equipment and analysis tools used in the course, the experimental portion of the lab course begins in week 4 with a single conventional "cookbook lab," in which students are given relatively detailed instructions to implement a gas pressure lab using Hexbugs™. This lab parallels earlier work by Prentis and is described in detail in Sec. III.[6]

The original research portion of the course begins in week 5 and continues for the remainder of the semester. Students are asked to choose at least three articles to read from a curated collection of experimental research papers, largely focused on statistical mechanics and prior experiments using Hexbugs™ or Squiggle-Balls™.[6,7,9–12,22] They are then asked to brainstorm potential research questions using Hexbugs™ and to list the ideas in a shared class resource document. A sampling of initial project ideas is shown in supplementary material Table 2.[3] After discussing and refining the ideas with the instructor, students work in pairs to select a research question and develop a formal research proposal, including a sketch of the proposed experimental setup and a discussion of what data are to be collected. For the remainder of the semester, the student pairs implement their original research projects with weekly feedback from their instructor. They iteratively design and build the experimental apparatus, collect and analyze data, and use their initial results to further refine the experiment, building key skills used in experimental physics research labs.[23]

In addition to the experimental research curriculum, scientific communication skills, such as reading and writing scientific papers, are taught throughout the course. This science communication curriculum is outlined in the third column of Table I. Students are first introduced to strategies for reading scientific papers and then practice this skill in the context of the mini-literature review required before selecting research topics. In week 5, the focus shifts to writing scientific papers. Students begin by reverse outlining a fairly conventionally written published paper. In this exercise, students identify the major components of the paper (Abstract, Introduction, Experimental Methods, etc.) and then outline the main arguments being made in each section. For example, the Introduction section contains a motivation for the work, a brief review of prior work in the area, and a clear statement of the purpose of the work described in the paper. This reverse outline then effectively serves as a scaffold for the remainder of the semester, as students write a formal scientific paper about their research project. Each subsequent week, students are required to write a section of their paper and to revise the section written the prior week, on which they have received detailed feedback. The completed manuscripts are then subjected to double-blinded peer review. During this review process, students learn a second, often overlooked, form of scientific communication, that of writing a constructive review. This exercise is supported by a set of "instructions for reviewers," modeled after those provided by physics journals (see supplementary material Appendix 1[3]), samples of high-quality reviews, and an in-class discussion of sources of bias in reviews.[25,26] The semester ends with students revising their manuscripts and writing formal responses to the reviews before submitting their final papers to their instructor for grading. In this manner, over the course of the semester, students refine their scientific writing skills while experiencing the entire life-cycle of publishing a paper: from performing the experiments to writing the paper and the review-revise-and-resubmit cycle of submitting a manuscript for publication.

The structure of this pandemic-inspired, distance lab course is intended to prepare—and hopefully to inspire—students to engage in independent research, in faculty-led research labs, summer internship programs, or their future careers. The intention of the course is to achieve all six laboratory learning outcomes outlined by the AAPT (see supplementary material Table 1[3]) developing key experimental and data analysis skills alongside learning to read and write scientific papers.[2]

III. GAS PRESSURE LAB

In order to familiarize students with the necessary experimental and data analysis skills before embarking on original research projects, students were required to adapt the "pressure fluctuation machine" experiments described by Prentis, replacing Prentis's Squiggle-Balls™ with Hexbugs™.[6] This statistical mechanics experiment enables a quantitative, macro-scale exploration of the ideal gas law by placing a movable piston between two "gasses" of differing concentrations of Hexbugs™, enabling students to explore the effects of mechanical interaction of the gas molecules (Hexbugs™) with the moveable wall.

In the spirit of "distance labs" meant to be conducted at home, the experimental apparatus is constructed using a collection of Hexbug Nanos™ that were mailed to the students, a smartphone, and items commonly found at home; the

materials provided to the students are listed in supplementary material Table 3.[3] Hexbug Nanos™ are small (7.2 g), battery-powered robots driven by an internal motor that vibrates the bugs' 12 flexible legs at about 100 Hz.[27] This rapid repeated motion allows the Hexbugs™ to move in a semi-random manner, such that a collection of Hexbugs™ can be approximated as a macroscopic gas.[4,8,12] The details of the apparatus varied slightly from student to student based on materials available; a typical setup is described here. A rectangular box (in this work, 32 × 21 cm^2) is placed on a flat, level surface and divided by a sliding wall positioned perpendicular to the length of the box, as shown in Fig. 1. The wall must be lightweight, yet rigid enough to prevent bending or twisting when impacted by the Hexbugs™; stacked bamboo skewers with the top and bottom skewers protruding through horizontal slits in the sides of the box, worked well and allowed the wall to slide along inside the box.[28] With collections of Hexbugs™ placed on either side of the wall, the apparatus functions as a model of a movable piston placed between two different gasses. To disrupt the tendency of the Hexbugs™ to become trapped in corners or to follow the walls of the box, small rounded cardboard barriers were placed in the corners to redirect the Hexbugs™ away from the walls.

At the start of each experiment, the wall was positioned at the center of the box at the $x = 0$ position, as shown in Fig. 1(b), such that the left and right chambers started off with the same area: $A_L(t=0) = A_R(t=0)$. N_L Hexbugs™ were then introduced to the left chamber and N_R Hexbugs™ to the right chamber, and the system was allowed to equilibrate. As the Hexbug™ "gas molecules" collided with the piston, the motion of the piston was video-recorded using a smartphone and subsequently analyzed using the video tracking software Tracker to obtain the position x(t) of the wall as a function of time.[29] In a typical experiment, the position of the wall was measured every 0.3 s. At each timepoint, the concentration $n_k(t)$ of the two-dimensional Hexbug™ gas can be calculated

$$n_k(t) = N_k/A_k(t), \quad \text{for } k \in \{L, R\}, \tag{1}$$

where the area $A_k(t)$ of the box is determined from the measurement of the position of the wall x(t).

The dynamics of the wall were tracked for three concentrations of the Hexbugs™. In two of the experiments, the starting concentrations of the Hexbug™ gasses on the left and right of the wall were equal ($n_L(t=0) = n_R(t=0)$), each chamber having the same numbers of Hexbugs™: ($N_L = 2$, $N_R = 2$) and ($N_L = 5$, $N_R = 5$). In the third experiment, the starting concentrations of the Hexbug™ gasses were uneven with differing numbers of bugs in each chamber ($N_L = 3$, $N_R = 2$).

The equilibrium state of this system can be predicted by the molecular form of the ideal gas law

$$PV = Nk_BT, \tag{2}$$

where P, V, and T are the pressure, volume, and temperature of the gas, respectively. N is the number of molecules, and k_B is Boltzman's constant. In our experiment, the temperature of the Hexbug™ gasses is constant because the average speed of the Hexbugs™ is constant. The pressure P_k exerted by each Hexbug™ gas on the center piston is, therefore, determined by the concentration n_k of the two-dimensional gas

$$P_k = n_k k_B T, \quad \text{for } k \in \{L, R\}. \tag{3}$$

The mean position of the piston in this system is at the point of mechanical equilibrium, when the pressures on the wall from the left and from the right are equal, or, equivalently, when the concentrations of the Hexbug™ gasses on the two sides of the wall are equal.

For each of the three initial configurations, sample student data (collected at home) are shown in Fig. 2, along with the mean and standard deviation of the wall position during a single experimental run. When the initial Hexbug™ gas concentration was the same on the left and right sides of the wall, the average position of the wall remained roughly at the origin, as expected. Furthermore, as the number of Hexbugs™ in the two chambers increased (while maintaining equal numbers of Hexbugs™ on both sides), the standard deviation of the wall position decreased because the displacement of the wall resulting from each Hexbug™ collision was more frequently offset by an opposing collision on the other side of the wall.[6]

In the ($N_L = 3$, $N_R = 2$) case, the initial concentration of the Hexbug™ gas was 33% greater on the left side of the wall than on the right side, so the greater number of collisions of Hexbugs™ into the left side of the wall moved the wall to the right. Remarkably, even with such small numbers

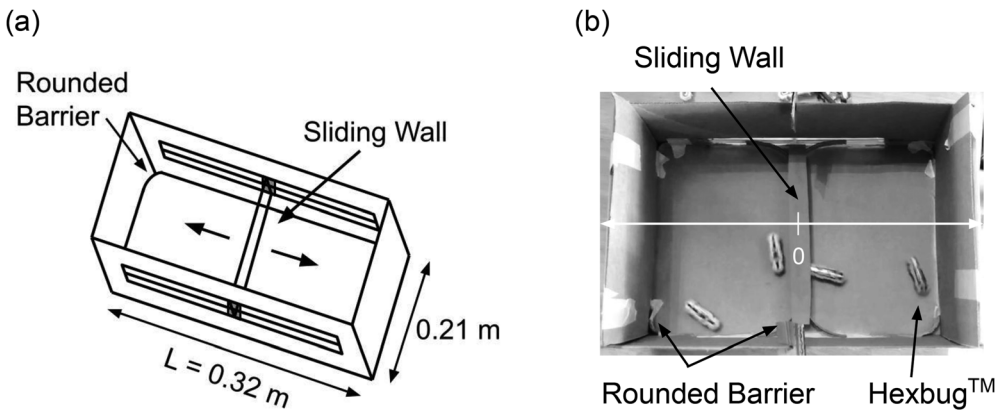

Fig. 1. 3D (a) and top (b) views of the experimental setup. A lightweight but rigid moveable wall is suspended from parallel slits and can slide along the length of the box. A coordinate system is defined such that the x-axis (white line in (b)) runs parallel to the length of the box with the origin ($x = 0$) defined to be in the center of the box. A collection of Hexbugs™ is placed on each side of the wall with N_L Hexbugs™ on the left side of the wall and N_R Hexbugs™ on the right.

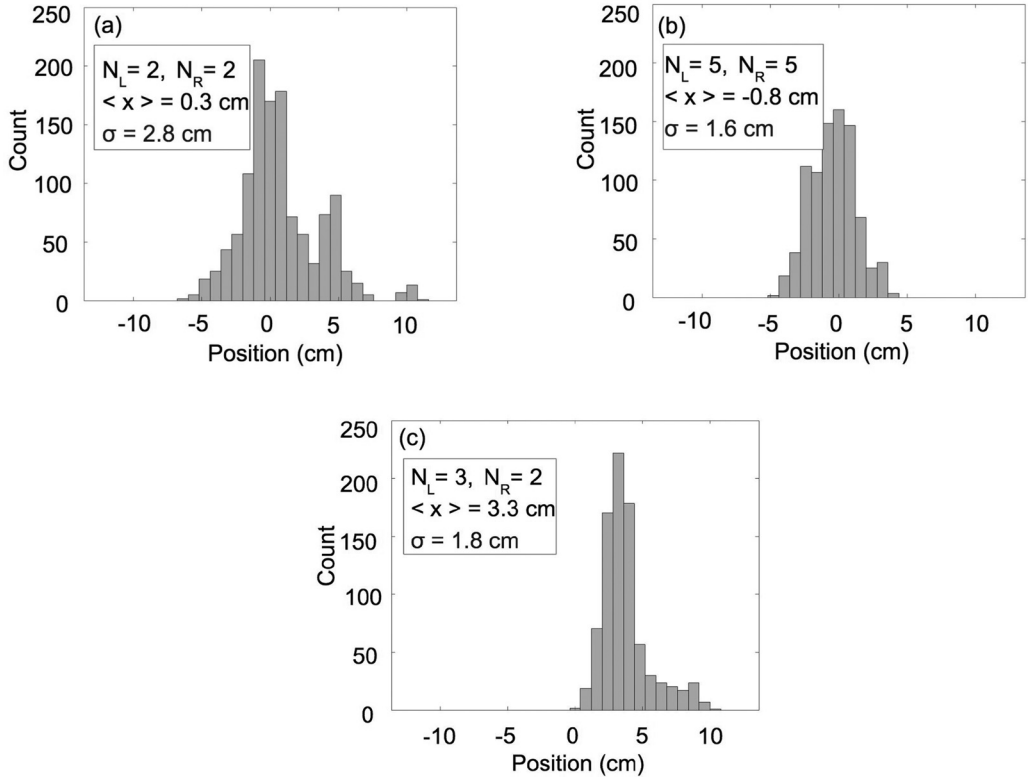

Fig. 2. Each histogram shows for N_L Hexbugs^{TM} in the left chamber of the gas pressure apparatus and N_R Hexbugs^{TM} in the right chamber, how many times the wall was measured to be in a given location during a single experimental run. All three experiments were conducted by the same student. In all cases, the position $x = 0$ is the initial position of the wall, when both chambers are of equal area. The mean $\langle x \rangle$ and standard deviation σ of the position of the wall are given for each experiment.

of "gas molecules," at the conclusion of the experiment, the concentration of the two Hexbug^{TM} gasses was nearly identical ($0.0074\,cm^{-2}$ on the left and $0.0075\,cm^{-2}$ on the right). This experiment was later repeated by the authors with higher numbers of Hexbugs^{TM} ($N_L = 3$, $N_R = 4$), similar results were obtained with the wall moving to the left until the concentration of the two gasses equilibrated, and the gas pressure in both chambers was the same.

While the mechanical force exerted by collisions of gas molecules with their container can be difficult to observe directly, this macro-scale Hexbug^{TM} gas model enables students to directly observe the effect of collisions of the Hexbug^{TM} gas molecules with a piston and permits a quantitative exploration of the ideal gas law. The simple, build-it-yourself experimental setup allows students to develop experimental design and to build skills while reinforcing basic data analysis techniques. The data in Fig. 2 illustrate the robustness of this experiment to somewhat typical weaknesses in a student-driven, at-home experimental measurement, including an implausibly low number of gas molecules and differing experimental durations between the three test cases. Also, the histograms in Fig. 2 correspond to the entire movement of the wall from the start of the experiment to the end. Consistent with the student's procedure, we have not removed the data corresponding to the transient regime in which the wall moves from its initial position to a position close to equilibrium, illustrating that the average wall position $\langle x \rangle$ is barely affected by the transients. Furthermore, these shortcomings can be discussed in class and are useful for the development of students' experimental skills through the critical assessment of their experimental design. This simple experiment is also a good springboard for students to brainstorm future work that builds on this experiment. For example, they could choose to address the experiment's limitations or to further investigate phenomena that they have observed such as the change in the standard deviation of the wall position as the number of Hexbugs^{TM} is varied.

IV. MODELING ELECTRICAL RESISTANCE AND CONDUCTION

Students developed a wide variety of research projects based on the initial brainstorming of ideas shown in Table II of the supplementary material.[3] In this section, we focus on one specific project, the modeling of electrical conduction, and exploration of the Drude model, which illustrates how a

Table II. Dependence of relaxation time, mean free path, and carrier mobility on scattering site density. Carrier mobility values were extracted from the slopes of the linear fits in Fig. 6, while the relaxation times and mean free paths were obtained from by-hand analysis of the individual video frames (running at 30 frames/second) as the Hexbug^{TM} moves through the experimental setup.

Density of scattering sites	Scattering site spacing (cm) ± 0.1 cm	Relaxation time τ (s) ± 0.03 s	Mean free path l (cm) ± 0.1 cm	Carrier mobility, μ_d (s) ± 0.005 s
Low	12.5	0.95	11.8	0.11
Medium	10	0.73	11.5	0.09
High	8.5	0.43	7.5	0.08

macroscopic experiment can be used to deepen students' understanding of a microscopic phenomenon.

The Drude model, proposed by German physicist Paul Drude in 1900, uses ideas from classical mechanics to describe electrical conduction. The model describes metals as an assembly of atoms with valence electrons that behave similarly to a gas. These conduction (valence) electrons are modeled as "free charges" that are randomly scattered as they move about in the metal with mean speed u; see Fig. 3(a). We note that while Drude attributed scattering of the conduction electrons to collisions with the lattice ions, quantum mechanics has shown that this is not the case and that scattering of the conduction electrons is largely due to impurities or phonons. We will come back to this point at the end of this section.

With no externally applied field, the average velocity of the conduction electrons is zero. Because there is no net movement of the electrons in any one direction, there is no net charge flow. However, in the presence of an applied external electric field, the randomly scattering conduction electrons are accelerated between collisions by the resulting electric force and acquire a net "drift velocity" in the direction of the electric force; see Fig. 3(b). The drift velocity $\vec{v}_d$ is defined as the instantaneous velocity in the direction of the electric force, averaged over many conduction electrons.[31]

The relationship between the drift velocity and the applied field can be obtained by following the derivation by Kasap.[31] Assume an electric field $\vec{E}$ is applied to a metal in the $-$x direction, as in the schematic in Fig. 3(b). To calculate the drift velocity of an ensemble of N conduction electrons, first consider the velocity $\vec{v}_i(t)$ of the i-th electron at time t. If the last scattering event experienced by the i-th electron occurred at time $t_i < t$, then during the time interval $t - t_i$, the electron experiences an acceleration $\vec{a}$ in the +x-direction due to the electric field

$$\vec{a} = e\,E/m_e\hat{x}, \tag{4}$$

where E is the magnitude of the field. E and m_e are the magnitudes of the charge and the mass of the electron, respectively. If $\vec{u}_i(t_i)$ is the velocity of the i-th electron resulting from the random scattering event at time t_i, then the velocity of the electron at time t is

$$\vec{v}_i(t) = \vec{u}_i(t_i) + e\,E/m_e(t - t_i)\hat{x}. \tag{5}$$

The Drude model assumes that a collision can scatter an electron in any direction and electrons emerge from a collision with speed u that only depends on the local temperature of the metal, so the velocity $\vec{u}_i(t)$ averaged over many electrons is zero. Hence, the drift velocity $\vec{v}_d$, which is defined as the instantaneous velocity averaged over all of the conduction electrons, is

$$\vec{v}_d = \frac{1}{N}\sum_{i=1}^{N}\vec{v}_i(t) = e\,E/m_e\langle t - t_i\rangle\,\hat{x}. \tag{6}$$

Following the derivation by Kasap, $\langle t - t_i\rangle$ is the average free time between collisions for N electrons, which is equal to the mean free time τ, defined as the mean time between collisions.[32] Hence, the magnitude of the drift velocity can be written as

$$v_d = (e/m_e)\,E\,\tau = \mu_d\,E, \tag{7}$$

where μ_d is the drift mobility (commonly called "carrier mobility"), defined as

$$\mu_d = (e/m_e)\,\tau. \tag{8}$$

The above derivation uses the definition of the drift velocity as the instantaneous velocity in the direction of the electric force, averaged over many conduction electrons. Alternatively, the drift velocity can be determined by focusing on the motion of a single conduction electron in the presence of an applied electric field over a time $\Delta t \gg \tau$; see Fig. 3(b). After many scattering events during the time interval Δt, the electron is displaced by a net distance Δx in the x-direction. Thus, the effective velocity at which the electron drifts in the x-direction is

$$\vec{v}_{eff} = \Delta x/\Delta t\,\hat{x}, \tag{9}$$

which is a time averaged velocity for a single electron over many scattering events. Under steady state conditions ($\Delta t \gg \tau$), the drift velocity and the effective velocity are equivalent.[33]

The distance equivalent to τ (commonly called the "relaxation time") is the mean free path, ℓ, defined as the mean distance traveled by the electrons between scattering events. Hence, the mean speed u between scattering events is

$$u = \ell/\tau. \tag{10}$$

In contrast to the drift velocity, the mean speed is assumed in the Drude model to be independent of any external electric field; see the discussion on the assumptions of the model below. The values of the drift mobility, relaxation time, and mean free path are determined by the properties of the material.

In the at-home experimental setup, electrical conduction in a metal is modeled using a long rectangular cardboard box with scattering sites constructed from cardboard rings arranged in a 2D cubic array and Hexbugs™ as the conduction electrons, see Fig. 4. Three different scattering site spacings were tested (see the caption of Fig. 4). In this macroscopic model of conduction, the electric field is modeled by the gravitational field. A difference in potential is applied by raising one end of the box by height h such that the floor of the box is at an angle θ relative to the horizontal plane. Defining a coordinate frame such that the x-axis is parallel to the length of the box as shown in Fig. 4, the resulting gravitational field $\vec{\mathcal{E}}$ along the length L of the box is

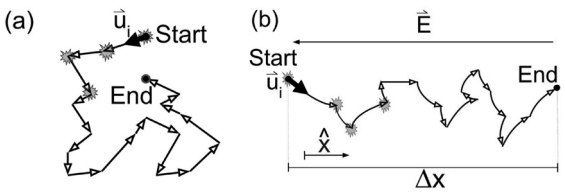

Fig. 3. The Drude model-based visualization of motion of a conduction electron in a metal (Ref. 30). (a) In the absence of an electric field, a conduction electron moves through the metal with average speed u between random scattering events, such that the time-averaged velocity of the electron is zero. The first four scattering events are marked with gray stars. (b) When an external electric field $\vec{E}$ is applied in the $-$x direction, the conduction electron accelerates in the +x direction between scattering events. Over a time interval Δt, the electron drifts a distance Δx in the +x direction.

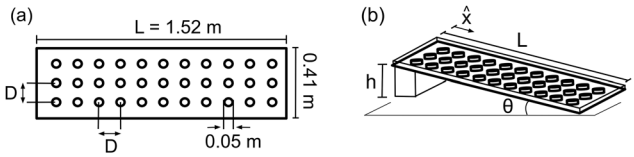

Fig. 4. The experimental setup used in the Drude model experiments with top (a) and 3D (b) views. The circles are cardboard rings (the scattering sites) arranged in a square array with center-to-center distance D. Each ring has a diameter of 5 cm. Three different scattering site densities were used in the experiments: low density (D = 12.5 cm, 3 × 11 array of scattering sites, as shown in (a)), medium density (D = 10 cm, 4 × 14 array of scattering sites), and high density (D = 8.5 cm, 5 × 17 array of scattering sites). The dimensions of the Hexbug Nano^{TM} "electrons" are 4.5 × 1.4 cm^2.

$$\vec{\mathcal{E}} = V_g/L\,\hat{x} = g\,h/L\,\hat{x} = g\sin\theta\,\hat{x}, \tag{11}$$

where V_g is the gravitational potential and g is the acceleration due to gravity. Note that, in contrast to the movement of electrons in the opposite direction to an electric field, Hexbugs^{TM} drift in the same direction as the gravitational field $\vec{\mathcal{E}}$ along the length of the box.

When released into the experimental setup, Hexbugs^{TM} move about the box with mean speed u, randomly scattered by collisions with the rings. When the box is leveled ($\theta = 0°$), such that there is no applied field, there should be no net movement of the Hexbugs^{TM} in any direction, such that the time-averaged velocity of the bugs is zero. When one end of the box is raised, creating a gravitational potential, the Hexbugs^{TM} are accelerated between collisions by the resulting gravitational field $\vec{\mathcal{E}}$ and acquire a net drift velocity in the direction of the field. Figure 5 shows the path of a representative Hexbug^{TM} with and without an applied field.

The relationship between the drift velocity of a collection of N Hexbugs^{TM} and the applied field $\vec{\mathcal{E}}$ can be derived following the analysis used for the Drude model. First, consider the velocity $\vec{v}_i(t)$ of the ith Hexbug^{TM} at time t. If the Hexbug^{TM} of mass m_H moves freely in the gravitational field

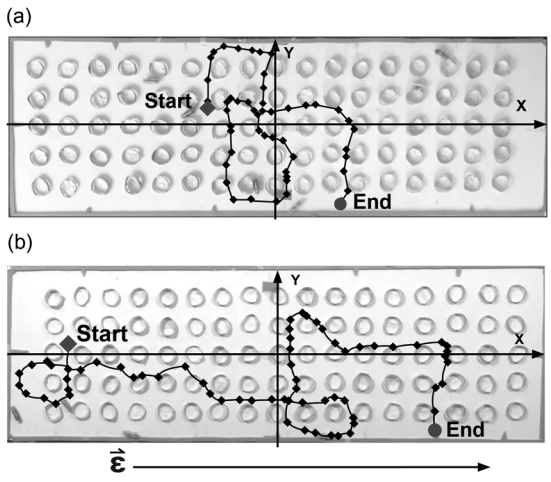

Fig. 5. Movement of a Hexbug^{TM} through the experimental setup with (a) the box leveled ($\theta = 0°$) and (b) the left side of the box raised relative to the right side ($\theta = 19°$) to create an external field $\vec{\mathcal{E}}$. The lines show the path of one of the Hexbugs^{TM} over time. Black squares indicate the position of the Hexbug^{TM} measured using the tracking software Tracker (Ref. 29), which analyzed every sixth frame of the 30 frames/second video; the connecting lines are guides to the eye. The track is overlaid on a photo of the box, in which several Hexbugs^{TM} are visible.

$\vec{\mathcal{E}}$ applied along the length of the box, then the bug experiences an accelerating force $\vec{F}$,

$$\vec{F} = m_H\vec{\mathcal{E}} = m_H\,g\sin\theta\,\hat{x}. \tag{12}$$

If the last collision of the Hexbug^{TM} with a scattering site occurred at time $t_i < t$, then during the time interval $t - t_i$, the Hexbug^{TM} experiences an acceleration $\vec{a}$ in the +x-direction due to the field

$$\vec{a} = \vec{F}/m_H = \vec{\mathcal{E}} = g\sin\theta\,\hat{x}. \tag{13}$$

Hence, the velocity of the Hexbug^{TM} at time t is

$$\vec{v}_i(t) = \vec{u}_i(t_i) + \vec{\mathcal{E}}(t - t_i), \tag{14}$$

where $\vec{u}_i(t_i)$ is the starting velocity of the Hexbug^{TM} resulting from the random scattering event at time t_i. Assuming that a collision with a scattering site can scatter a Hexbug^{TM} in any direction, the velocity $\vec{u}_i(t_i)$ averaged over many Hexbugs^{TM} is zero. Hence, as in the Drude model derivation, the drift velocity $\vec{v}_d$ is

$$\vec{v}_d = \frac{1}{N}\sum_{i=1}^{N}\vec{v}_i(t) = \vec{\mathcal{E}}\,\langle t - t_i\rangle = \vec{\mathcal{E}}\,\tau = \mu_d\,\vec{\mathcal{E}}, \tag{15}$$

where τ is the mean free time between scattering events, averaged over all N Hexbugs^{TM}.[32] Using the conventional definition of the drift mobility, we then have

$$\mu_d = \tau \tag{16}$$

for Hexbugs^{TM} moving freely in the gravitational field $\vec{\mathcal{E}}$.

However, in practice, the Hexbugs^{TM} does not move freely in this gravitational field, as the gravitational force is offset by a substantial frictional force between the legs of the Hexbug^{TM} and the box. The slip-stick dynamics of the Hexbug^{TM} legs are complex enough to require numerical simulation and are not easily modeled analytically.[15] In this work, we introduce a phenomenological scaling parameter, α (where $\alpha < 1$), to account for the reduction in the net force acting in the direction of the gravitational field[34]

$$\vec{F}_{net} = \alpha\,m_H\,\vec{\mathcal{E}} = \alpha\,m_H\,g\sin\theta\,\hat{x}. \tag{17}$$

With this adaptation, the magnitude of the drift velocity of the Hexbugs^{TM} becomes

$$\vec{v}_d = \alpha\,\vec{\mathcal{E}}\,\tau = \mu_d\,\vec{\mathcal{E}}\,, \tag{18}$$

where the carrier mobility, consequently, is reduced by the scaling factor

$$\mu_d = \alpha\tau. \tag{19}$$

In all experiments, six spatially separated Hexbugs^{TM} were simultaneously released in the box, starting from near the raised end, and allowed to interact with the scattering sites. The movement of the Hexbugs^{TM} was recorded in a video using a smartphone, and the video was subsequently analyzed using the software Tracker to obtain the movement of each Hexbug^{TM}.[29] In the analysis, we measured the effective velocity $\vec{v}_{eff}$ at which a Hexbug^{TM} drifts in the x-direction

(Eq. (9)). As in the Drude model of electrical conduction discussed above, under steady state conditions ($\Delta t \gg \tau$), this time averaged effective velocity for a single Hexbug^{TM} over many collisions is equivalent to the drift velocity.

With six Hexbugs^{TM} in each experiment, trials were run at each of eight different angles of the box and for three different densities of scattering sites. The resulting mean drift velocities are shown in Fig. 6. Within the uncertainty of the measurements, the results are consistent with the prediction of Eqs. (7) and (18) that the magnitude of the drift velocity should scale linearly with the magnitude of the applied field $\vec{\mathcal{E}}$. Hence, the Hexbug^{TM} experiment provides a clearly visible, macro-scale model of carrier transport in a wire that is consistent with the Drude model.

The model can be used to illustrate the effect of material properties on electrical transport as well. For example, as the density of scattering sites increases (i.e., the spacing between the rings in the experimental setup decreases), the relaxation time τ should decrease. Examining trials for each of the three scattering site densities, τ was determined by measuring the mean free time between collisions. Similarly, mean free path ℓ of the Hexbugs^{TM} between scattering processes was determined by measuring the mean distance between collisions. Table II shows the measured mean relaxation time and mean free path for each scattering site density, along with the carrier mobilities extracted from Fig. 6. As expected, both the relaxation time and mean free path decreased with increasing scattering site density, as did the carrier mobility, consistent with the predictions of Eq. (19).

Using the measured relaxation times given in Table II, the drift velocities for all three scattering site densities are plotted together in Fig. 7 as a function of the product of the magnitude $\mathcal{E}$ of the applied field and the relaxation time τ. Remarkably, as predicted in Eq. (18), the drift velocities appear to scale linearly with $\mathcal{E}\tau$, allowing for some scatter in the measurements, providing a dramatic macro-scale visualization of the Drude model. Furthermore, the slope of the plot provides a quantification of the phenomenological scaling parameter, $\alpha = 0.11$, introduced in Eq. (17) to account for the complex friction dynamics impacting the motion of the Hexbugs^{TM} in the gravitational field.[35]

The Drude model makes several key assumptions that must be taken into account when constructing this

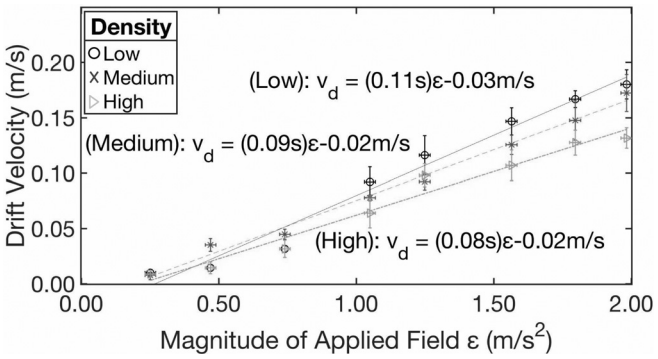

Fig. 6. Mean Hexbug^{TM} drift velocity, averaged over six trials at each point vs the magnitude $\mathcal{E}$ of the applied field along the length of the box. Vertical error bars show the standard deviation of the mean of the six trials. The field was varied by changing the angle at which the box is tilted ($\theta \in \{1°, 3°, 4°, 6°, 7°, 9°, 11°, 12°\}$), as in Eq. (11). Experiments were run at three different scattering site densities defined in the caption of Fig. 4. Lines are best fits to the points for each density.

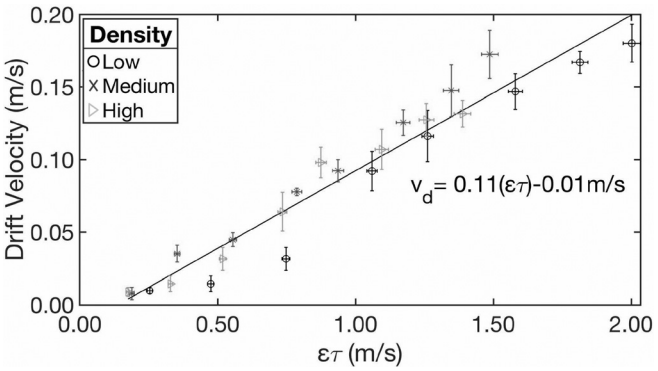

Fig. 7. Mean Hexbug^{TM} drift velocity, averaged over six Hexbugs^{TM} at each point, vs the product of the magnitude $\mathcal{E}$ of the applied field and the measured relaxation time τ for the corresponding scattering site density. Vertical error bars show the standard deviation of the mean of six trials. The dataset contains drift velocities measured using the three different scattering site densities, and hence, three differing relaxation times, given in Table II. Line is the best fit to the points.

macroscopic model system.[31,36,37] First, the model assumes that conduction electrons do not interact with each other and are not influenced by the lattice ions between collisions.[38] Hence, in the absence of an electric field, a conduction electron moves in a straight line path between collisions. This assumption is satisfied in the experimental setup by using few enough Hexbugs^{TM} (typically six) that they do not collide with each other during the experiments. Second, when the electrons are scattered, they lose all of the energy gained from an applied field and are scattered in a random direction. This assumption is satisfied in our Hexbug^{TM} model, as the observed drift velocity does not increase over time. Finally, the Drude model assumes that the relaxation time τ is independent of the applied field, because the mean speed u is much greater than the magnitude of the drift velocity ($u \gg |\vec{v}_d|$); this constraint puts an upper limit on the slope of the box. The mean speed obtained from the data in Table II is noisy but of the order of $u = 0.15$ m/s, while the measured drift velocities (see Fig. 6) range in amplitude from 0.01 to 0.18 m/s, such that many of the experimental trials violate this assumption of the model ($u \gg |\vec{v}_d|$). Despite this limitation, Fig. 7 shows that the data collected using the macro-analogue are remarkably consistent with the Drude model.

Furthermore, there is an important conceptual limitation to both the Drude model and the Hexbug^{TM} analogue described in this work, which should be explicitly considered. When the Drude theory was originally formulated, it was assumed that electrons scattered from the periodic lattice of ions. However, quantum mechanical models eventually showed that electron wave functions accommodate the periodic lattice, and scattering occurs only from defects in the periodicity such as impurities and phonons. In this experiment, the Hexbugs^{TM} behave classically and scatter even from a regularly spaced array, which could lead students to an incorrect understanding of electron conduction. When implemented in an instructional setting, the Hexbug^{TM} experiments could be improved by arranging the scattering sites (cardboard rings) randomly, rather than in an array, and instructors should accompany this Drude model-based experiment with a discussion of the modern understanding of electrical conduction.

In conclusion, modeling electrical conduction using Hexbugs^{TM} on a tilted plane provides a visible-scale

analogue to the Drude model of electrical conduction. Students are able to see the interactions of the electrons (Hexbugs^{TM}) with the scattering sites and appreciate the difference between the mean speed u and the drift velocity. Furthermore, it is readily apparent why changing material properties, such as the density of scattering sites, affects the mean free path and relaxation time of electrons, and consequently, the carrier mobility and electrical conductivity.

V. CONCLUSIONS

As illustrated by both the gas pressure and electrical conduction experiments, collections of Hexbugs^{TM} can be used to develop simple but effective macro-scale models of common micro-scale phenomena in statistical mechanics and electronics. These macro-scale analogues are consistent with established physical models (here, the ideal gas law and the Drude model) and enable students to visualize the underlying physical behaviors that are otherwise largely invisible, such as the mechanical forces exerted by gas molecules on their containers and the conduction of electrons through a metal.

Paradoxically, despite having shifted to online labs as a pandemic-inspired exigency, we found that the necessary de-emphasis on the use of sophisticated scientific equipment enabled greater focus on the learning outcome focus areas recommended by the AAPT.[2] Of the six AAPT-recommended focus areas listed in supplementary material Table 1,[3] five of the areas were robustly met to the "advanced level" standard in the AAPT guidelines with the online lab course, while the sixth area "developing technical and practical laboratory skills" was met to the "introductory level" standard due to the inability to use advanced laboratory equipment. Student comments on end-of-semester learning evaluations and feedback from the lab teaching assistants at the end of the semester were consistent with these observations with almost all of the students highlighting the positive impact of pursuing an independent research project of their choosing and their perceived gains in experimental skills, while lamenting the lack of access to conventional scientific grade equipment. Consistent with the thesis of Fox *et al*. that "the move to remote/hybrid teaching may be a unique opportunity to transform the lab course,"[1] as we transition back to in-person labs, we hope to use the lessons learned from the pandemic lab experience to achieve the best of both worlds: a redoubled focus on developing experimental research skills, combined with building students' expertise with standard scientific instrumentation.

ACKNOWLEDGMENTS

The authors wish to thank the students, teaching assistants, and writing partners of the Fall 2020 Foundations of Modern Physics course at Pomona College for their creativity and investment in this work, including the sample project ideas listed in supplementary material Table 2 (Ref. 3). The authors would also like to thank David Haley, Senior Laboratory Technician, for assembling the lab kits and distributing them to students spread around the globe. Kara Wittman provided invaluable advice in designing the scientific writing portion of the curriculum, and the authors are indebted to the members of the Research and Instructional Technology Group at Pomona College for their guidance in transitioning effectively to online learning. The authors wish to thank all for learning in and making a success of a challenging pandemic semester.

[a]G. DiBari and L. Valle contributed equally to this paper.
[b]Electronic mail: lwva2018@mymail.pomona.edu, ORCID: 0000-0002-1514-044X.
[c]ORCID: 0000-0003-3264-5228.
[d]ORCID: 0000-0003-0122-8915.
[e]ORCID: 0000-0001-8204-1137.

[1]M. F. J. Fox, A. Werth, J. R. Hoehn, and H. J. Lewandowski, "Teaching labs during a pandemic: Lessons from Spring 2020 and an outlook for the future," arXiv:2007.01271 (2020).
[2]AAPT Committee on Laboratories, *AAPT Recommendations for the Undergraduate Physics Laboratory Curriculum* (AAPT, College Park, MD, 2015).
[3]See the supplementary material at https://www.scitation.org/doi/suppl/10.1119/5.0087142 for AAPT recommended laboratory learning outcome focus areas, sample student project ideas, a list of lab supplies, and the Guidelines for Reviewers provided to students.
[4]C. Tapia-Ignacio, L. L. Gutierrez-Martinez, and M. Sandoval, "Trapped active toy robots: theory and experiment," J. Stat. Mech. **2021**(5), 053404.
[5]Squiggle-Balls^{TM} are inexpensive, baseball-sized toy balls that use an asymmetric rotor to roll around.
[6]J. J. Prentis, "Experiments in statistical mechanics," Am. J. Phys. **68**(12), 1073–1083 (2000).
[7]T. Gfroerer and K. Rathbun, "Squiggle ball capture: A simple, visual kinetic theory experiment," Phys. Teach. **45**(6), 344–347 (2007).
[8]To first order, as described by Sánchez and Díaz-Leyva, "On smooth, level surfaces they [Hexbugs Nano^{TM}] move almost exactly along a straight line along their lengths and in the direction of their 'heads' with negligible rotational motion as long as they do not collide," and on collision are randomly scattered; see Ref. 12. There are relatively minor second-order stochastic effects due to surface roughness and deterministic effects, including an asymmetry in their center of mass and Newton's third law reaction to the clockwise rotation of the motor; the motion is characterized in detail in Refs. 4 and 12. However, these second order effects are not observed to affect the results in this work.
[9]L. Giomi, N. Hawley-Weld, and L. Mahadevan, "Swarming, swirling and stasis in sequestered bristle-bots," Proc. R. Soc. A **469**(2151), 20120637 (2013).
[10]H. Li and H. P. Zhang, "Asymmetric gear rectifies random robot motion," Europhys. Lett. **102**(5), 50007 (p. 1–6) (2013).
[11]H. Li, X. Yang, and H. Zhang, "Symmetry properties of fluctuations in an actively driven rotor," Chin. Phys. B **29**(6), 060502 (2020).
[12]R. Sánchez and P. Díaz-Leyva, "Self-assembly and speed distributions of active granular particles," Physica A **499**, 11–19 (2018).
[13]O. Dauchot and V. Démery, "Dynamics of a self-propelled particle in a harmonic trap," Phys. Rev. Lett. **122**(6), 068002 (2019).
[14]M. Leoni *et al*., "Surfing and crawling macroscopic active particles under strong confinement: Inertial dynamics," Phys. Rev. Res. **2**(4), 043299 (2020).
[15]C. Gandra and P. Tallapragada, "Dynamics of a vibration driven bristlebot," paper presented at the ASME 2019 Dynamic Systems and Control Conference, 2019.
[16]A. Dirafzoon, E. Lobaton, and A. Bozkurt, "Exploration and topological mapping with Hexbugs^{TM}," in *Proceedings of the 14th International Conference on Information Processing in Sensor Networks*, New York, NY (IEEE, 2015), pp. 406–407.
[17]H. Löwen, "Inertial effects of self-propelled particles: From active Brownian to active Langevin motion," J. Chem. Phys. **152**(4), 040901 (2020).
[18]X. Yang, C. Ren, K. Cheng, and H. P. Zhang, "Robust boundary flow in chiral active fluid," Phys. Rev. E **101**(2), 022603 (2020).
[19]E. Zheng, M. Brandenbourger, L. Robinet, P. Schall, E. Lerner, and C. Coulais, "Self-oscillation and synchronisation transitions in elasto-active structures," arXiv:2106.05721 (2021).
[20]Wolfram Mathematica: Modern technical computing at <https://www.wolfram.com/mathematica/> (last accessed May 10, 2022).
[21]MATLAB-MathWorks at <https://www.mathworks.com/products/matlab.html> (last accessed May 10, 2022).
[22]M. A. Catipovic, P. M. Tyler, J. G. Trapani, and A. R. Carter, "Improving the quantification of Brownian motion," Am. J. Phys. **81**(7), 485–491 (2013).
[23]The student lab partners were geographically separated and working remotely during the pandemic under widely varying circumstances. Hence, the specifics of how the assignment was implemented varied between project teams. In some cases, both students in a team built the apparatus and compared design ideas and results. In other cases, one team member built the apparatus and the second team member participated in the experimental design, implementation, and data analysis remotely.

[24]C. Schmidl, see https://towardsdatascience.com/how-to-read-scientific-papers-df3afd454179 for "How to read scientific papers, medium" (last accessed January 5, 2022).
[25]A. Tomkins, M. Zhang, and W. D. Heavlin, "Reviewer bias in single- versus double-blind peer review," Proc. Natl. Acad. Sci. **114**(48), 12708–12713 (2017).
[26]M. Helmer, M. Schottdorf, A. Neef, and D. Battaglia, "Gender bias in scholarly peer review," eLife **6**, e21718 (2017).
[27]Robotics, HEXBUG Nano™ how it works, 2011 at <https://www.youtube.com/watch?v=dhRoqUkhbdU> (last accessed January 5, 2022).
[28]It is important that the wall does not rotate during collisions by the Hexbugs™. If this becomes a problem, a flat plate or cap can be added to the skewers just outside of the box to prevent rotation.
[29]Tracker video analysis and modeling tool for physics education at https://physlets.org/tracker/ (last accessed September 12, 2021).
[30]Drude originally attributed electron scattering to collisions with ions in the lattice, leading to the visualization shown in Refs. 31, 36, and 37. In reality, electrons are scattered from phonons and irregularly spaced defects.
[31]Safa Kasap, *Principles of Electronic Materials and Devices*, 4th ed. (McGraw Hill, New York, 2017).
[32]Please see p. 128 of Ref. 31 for a more detailed explanation, including a derivation of the equivalence of $\langle t - t_i \rangle$ and τ.
[33]The derivation of this result can be found in p. 132 of Ref. 31.
[34]At first glance, there is little reason to expect that a constant scaling factor can succeed as a rough proxy for such complex behavior. However, the experimental results in Figs. 6 and 7 suggest that this approach is adequate for describing the simple experiments in this work.
[35]We independently estimated α by examining an experimental run in which a Hexbug™ traveled approximately halfway down the box before colliding with a scattering site. From this, we extracted a value of $\alpha = 0.18$. This measurement was noisy and involved only a single trial, so this rough independent estimate is reasonably consistent with the more carefully obtained result of $\alpha = 0.11$ from Fig. 7.
[36]M. N. Rudden and J. Wilson, *Elements of Solid State Physics* (Wiley, New York, 1993).
[37]Neil W. Ashcroft and N. David Mermin, *Solid State Physics*, 1st ed. (Thomson Learning, Boston, 1976).
[38]When discussing this assumption of the Drude model, Ashcroft and Mermin add the caveat "… although the independent electron approximation [neglecting electron–electron interactions] is in many contexts surprisingly good, the free electron approximation [neglecting electron–ion interactions] must be abandoned if one is to arrive at even a qualitative understanding of much of metallic behavior" (see Ref. 37).

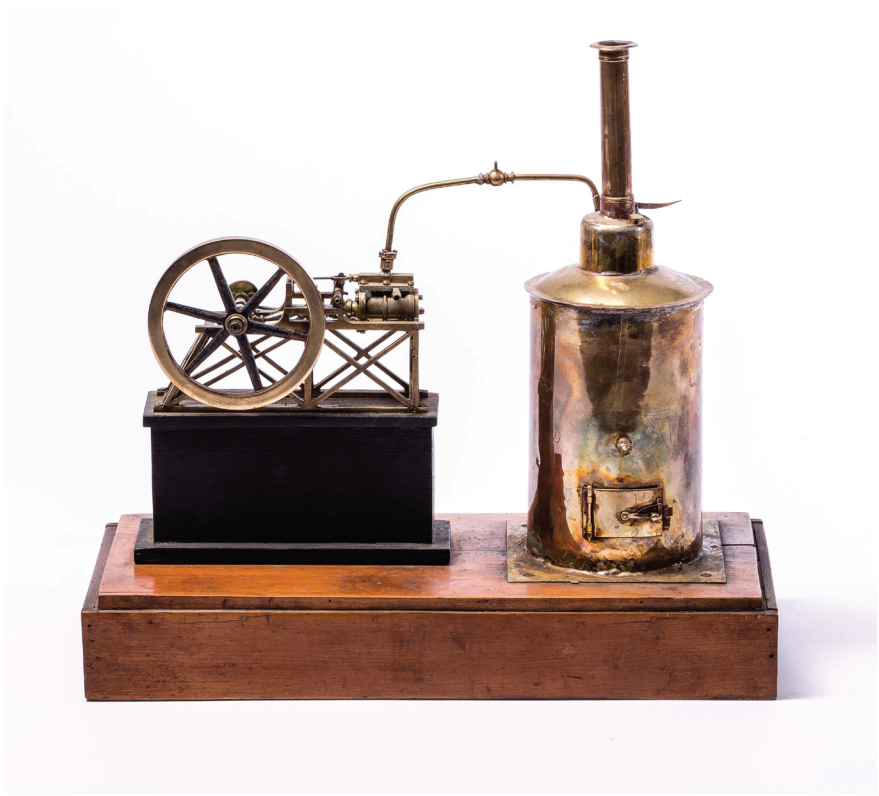

Steam Engine

The operation of the steam engine was a staple of the nineteenth century physics course. This beautiful example is probably pre-1900. The steam engine proper is the little cylinder in the middle with a slide valve at its back for admitting and exhausting the steam produced by the boiler at the right. The energy stored in the rotating flywheel is essential to keep the system running, and is part of the mechanism for converting the oscillating motion of the piston to rotational motion. This engine is in the collection of Amherst College. (Amherst College picture and text by Thomas B. Greenslade, Jr., Kenyon College)